Schiff-base [4]helicene Zn(ii) complexes as chiral emitters

Mariia Savchuk, Steven Vertueux, Thomas Cauchy, Matthieu Loumaigne, Francesco Zinna, Lorenzo Di Bari, Nicolas Zigon, Narcis Avarvari

ARTICLE

Schiff-base [4]helicene Zn(II) complexes as chiral emitters

Mariia Savchuk,[†,a] Steven Vertueux,[†,a] Thomas Cauchy,[a] Matthieu Loumaigne,[a] Francesco Zinna,[b] Lorenzo Di Bari,[b] Nicolas Zigon*[a] and Narcis Avarvari *[a]

Received 00th January 20xx,
Accepted 00th January 20xx

DOI: 10.1039/x0xx00000x

The controlled preparation of chiral emissive transition metal complexes is fundamental in the field of circularly polarized luminescence (CPL) active molecular materials. For this purpose, enantiopure Zn(II) complexes **1-2** based on a tetradentate salen ligand surrounded by [4]helicene moieties, together with the racemic counterpart **3**, have been herein synthesized. Chirality is primarily brought by chiral 1,2-cyclohexane-diamines. Alternatively, the achiral complex **4** based on *ortho*-phenylene-diamine has been prepared as well. Single crystal X-ray diffraction analyses have been performed on the helicenic intermediates **8** and **9** and complexes **1** and **4**. Complexes **1** and **4** display the typical tetradentate O,N,N,O coordination around Zn(II) characteristic of salen ligands, and bearing two [4]helicene moieties. The zinc complexes are luminescent in the visible range around 560 nm at room temperature in aerated solutions with QY reaching ca. 15% for a luminescence lifetime of 5.5 ns. The optical activities of these complexes have been assessed by CD and CPL, and compared to DFT calculations.

Introduction

Schiff base complexes derived from the salen ligand have been thoroughly explored for their unique properties.[1–3] Usually obtained by the condensation of a diamine with two equivalents of a salicylaldehyde derivative, they yield a versatile tetradentate ligand, that can be easily adapted in terms of steric hindrance and electronic properties. They attracted a particular deal of interest for their catalytic activity, in particular for epoxidation reaction with the well-known Jacobsen's catalyst based on a Mn(III)-salen complex, which was also successfully adapted for chiral catalysis.[4,5]

In addition to their use in catalysis, salen based complexes have drawn attention both for their magnetic properties,[6,7] especially when containing lanthanide ions,[8,9] or manganese (III),[10–12] and their emissive properties.[13–16] Noteworthy, Zn(II) and Ni(II)-salen have been incorporated in LED devices.[17–20]

Our group has a long-lasting interest for chiral materials,[21] and, therefore, developed several compounds using the helicenic scaffold, which is an *ortho*-fused polyaromatic moiety.[22] Helicenes and heterohelicenes are renowned for their large magnitude of chiroptical properties, such as optical rotation (OR), electronic circular dichroism (ECD), vibrational circular dichroism (VCD) and circularly polarized luminescence (CPL).[23,24] Moreover, their combination with metal complexes has been explored to yield phosphorescent compounds.[25–27] Accordingly, we have designed electro- [28] and photo-active [29–31] helicene and heterohelicene compounds and investigated their properties.

Herein, we describe the first enantiopure Zn(II)-salen-helicene complexes together with their photophysical and chiroptical properties, supported by TD-DFT calculations. Using Zn(salen) complexes for their luminescence properties is also strongly attractive due to the Zn(II) earth abundancy and low price compared to heavier metals.

Experimental

General procedures

All the solvents and precursors were commercially available and used without further purification. Infrared (IR) spectra were recorded in the solid state using a Bruker Vertex 70 spectrometer with Platinum ATR in the 400–4000 cm^{-1} range. ^{1}H, ^{13}C and 2D-NMR spectra were recorded on a Bruker Advance DRX 300 spectrometer operating at 300/500 MHz for ^{1}H and 75/125 MHz for ^{13}C. Chemical shifts are given in ppm relative to tetramethylsilane TMS and coupling constants J in Hz. Residual non-deuterated solvent was used as an internal standard.

Mass spectra were obtained either by the MALDI-TOF or FAB techniques by using a Bruker Biflex-IIITM apparatus, equipped with a 337 nm N_2 laser, by electron impact methods using a Thermo Electron Corporation TRACE-DSQ apparatus.

Lifetime measurements were performed on a modified Olympus IX73 microscope with a standard epi-fluorescence configuration. The chromophores (concentration 10^{-5} M) were excited with a 375nm pulsed laser diode with a pulse duration of 70ps. The laser beam was focused with a microscope objective (Olympus UPLSAPO x20 0.75NA). Excitation light was filtered via a dichroic beamsplitter (Semrock Di03-R405) and an emission filter (Semrock BLP01-405R-25). Single photons were

[a] *Univ Angers, CNRS, MOLTECH-Anjou, SFR MATRIX, F-49000 Angers, France. E-mail: nicolas.zigon@univ-angers.fr; narcis.avarvari@univ-angers.fr*
[b] *Dipartimento di Chimica e Chimica Industriale, Università di Pisa, via G. Moruzzi 13, 56124, Pisa, Italy.*
† These authors contributed equally to this work.

detected with an Avalanche PhotoDiode (PDM Micro Photon Devices) and the corresponding electrical pulses were sent to a TCSPC (Time-Correlated Single Photon Counting) Device (SPC 130-EM B&H). Fluorescence decays were analyzed with a homemade open-source software (https://github.com/MLoum/pySPC).

CPL measurements were carried out with a home-made spectrofluoropolarimeter.[32] The samples concentration was around $1 \cdot 10^{-1}$ M in THF for **1-2** and DMSO for **10-11** respectively. A 365 nm LED was used as the excitation source, employing a 90° geometry between excitation and detection. In the case of Zn-salen model compound, the excitation beam was linearly polarized on the detection plane, in order to avoid linear artefacts due to photoselection. Luminescence dissymmetry factors (g_{lum}) were calculated as $2(I_L-I_R)/ (I_L+I_R)$, where I_L and I_R are left and right circularly polarized components of the emission. The spectra are the average of 6 accumulations each. The theoretical spectra resulted from TD-DFT calculations using Gaussian with the PBE0 functional and a def2SVP basis set. The X-ray structure was used as a basis for atomic positions, which were further optimized.[33,34,35] 2-naphthylmethyltriphenylphosphonium bromide,[36] and 3-bromo-4-((tert-butyldimethylsilyl)oxy)benzaldehyde **5** [37] and model complexes **10-12** [38] were synthesized according to reported literature procedures.

Synthesis

2-bromo-4-(2-(naphthalen-2-yl)vinyl)phenoxy)(tert-butyl)dimethylsilane (6). 2-naphthyl-methyltriphenylphosphonium bromide (1.26 g, 2.61 mmol, 1 equiv.) was dissolved in 15 mL of dry THF under argon atmosphere. The mixture was cooled down to -78°C and then *n*BuLi (1.8 mL, 1.6M in hexane, 2.88 mmol, 1.1 equiv.) was added dropwise. After 10 min at -78°C, it was warmed to room temperature and stirred for 30 minutes. The mixture was cooled down again to -78°C and aldehyde **5** was added (0.82 g, 2.61 mmol, 1 equiv.). The mixture was stirred 10 minutes at -78°C, then warmed to room temperature and left at RT overnight. After filtration on Celite and concentration under vacuum, column chromatography (DCM : PE = 9:1) yielded **6** as a translucent oil (0.9 g, 79% mixture of isomers). ^{1}H NMR (300 MHz, $CDCl_3$): δ (ppm) 0.20 (s, 6H) 1.0 (s, 9H) 6.49 (d, J = 12.2 Hz, 1H) 6.66 (d, J = 12.2 Hz, 1H) 6.64 (d, J = 8.4 Hz, 1H) 7.05 – 7.00 (m, 1H) 7.47 – 7.29 (m, 4H) 7.77 – 7.60 (m, 4H). ^{13}C NMR (125 MHz, $CDCl_3$) δ (ppm) 181.22, 152.22, 151.75, 134.62, 133.88, 133.49, 132.62, 131.73, 129.96, 128.85, 128.77, 128.00, 127.96, 127.66, 127.60, 127.23, 126.82, 126.53, 126.09, 125.97, 123.41, 120.31, 119.79, 115.06, 77.47, 77.04, 76.62, 25.75, 18.39, -4.21. HRMS (FAB) m/z = 438.1024, theor. calc. 438.1015 (M+).

3-bromo-2-OTBDMS-[4]helicene (7). 6 (1.46 g, 3.32 mmol, 1 equiv.), iodine (0.87 g, 3.42 mmol, 1.1 equiv.) and propylene oxide (9.64 g, 166 mmol, 50 equiv.) were dissolved in toluene (650 mL), degassed thoroughly and placed in a photoreactor equipped with an immersion lamp (150 W). The mixture was irradiated for one night. After evaporation of the solvent and purification by column chromatography over SiO_2 (PE : EtOAc = 9.9 : 0.1) compound 7 was obtained as a yellow oil (0.77 g, 53%). ^{1}H NMR (300 MHz, $CDCl_3$): δ (ppm) 7.78 – 7.64 (m, 4H) 7.82 (d, J = 8.5 Hz, 1H) 7.92 (d, J = 8.5 Hz, 1H) 8.08 – 8.03 (m, 1H) 8.08 – 8.03 (m, 1H) 8.66 (s, 1H) 9.06 (d, J = 8.4 Hz, 1H). ^{13}C NMR (75 MHz, $CDCl_3$): δ (ppm) 150.97, 133.46, 132.61, 131.35, 130.50, 130.22, 129.71, 128.77, 127.74, 127.18, 126.98, 126.25, 126.16, 126.10, 125.96, 125.80, 116.66, 115.77, 77.51, 77.09, 76.66, 25.89, 18.58, -4.07. MS (MALDI-TOF) m/z = 437.1, theor. calc. 437.1 (M+H+).

3-cyano-2-hydroxy-[4]helicene (8). A microwave vial was charged with **7** (0.77 g, 1.76 mmol, 1 equiv.) and CuCN (0.79 g, 8.8 mmol, 5 equiv.). The vial was capped with PTFE septa and dry NMP (20 mL) was added. The reaction mixture was bubbled with Argon for 10 min, and then placed in a microwave reactor for 3 hours at 210 °C. After the reaction, an aqueous solution of NH_4OH was added and the product was extracted with EtOAc (3 x 100 mL). Organic phases were washed with brine and dried on $MgSO_4$. Column chromatography (DCM: MeOH = 9:1) yielded **8** as a dark crystalline powder (0.56 g, 71%). ^{1}H NMR (500 MHz, CD_3OD): δ (ppm) 7.68 – 7.56 (m, 3H), 7.79 – 7.74 (m, 2H), 7.91 (d, J = 8.5 Hz, 1H), 7.99 (dd, J = 7.9, 1.5 Hz, 1H), 8.25 (s, 1H), 8.57 (s, 1H), 8.97 (d, J = 9.3 Hz, 1H). ^{13}C NMR (125 MHz, CD_3OD): δ (ppm) 158.38, 144.48, 136.40, 135.71, 135.01, 134.47, 131.70, 130.28, 130.04, 128.26, 128.03, 127.93, 127.79, 127.30, 126.69, 126.56, 117.69, 112.87, 101.95. HRMS (FAB) m/z = 269.0832, theor. calc. 269.0841 (M+). IR: 3335-2718m, 2226m, 1654w, 1602m, 1534w, 1498w, 1450w, 1430 w, 1398 w, 1358 w, 1306 w, 1262 w, 1234 w, 1206 w, 1183 w, 1135 w, 1087 w, 1015 w, 891m, 827m, 795w, 775w, 747m, 699w, 643w, 619w, 583w, 539w, 499m, 451w, 404w. UV (MeOH, 10^{-5} M): λ_{max1} = 387nm, λ_{max2} = 290nm.

3-aldehyde-2-hydroxy-[4]helicene (9). 8 (1.1 g, 4.08 mmol, 1 equiv.) was dissolved in 250 mL of toluene under and DIBAl-H was added dropwise (1M/CH_2Cl_2, 6.2 mL, 6.2 mmol, 1.5 equiv.). The reaction mixture was stirred overnight and quenched with 100 mL H_2O at 0°C, 100 mL of 10% HCl solution and stirred 8h at RT. After extraction with dichloromethane (3 x 150 mL), the reunited organic phases were washed with water, dried on $MgSO_4$ and concentrated under vacuum. A yellow sticky solid **9** was obtained (0.59 g, 53%) after purification by column chromatography with DCM as eluent. ^{1}H NMR (300 MHz, $CDCl_3$): δ (ppm) 7.82-7.68 (m, 3H), 7.96-7.93 (m, 1H), 8.1-8.01 (m, 2H), 8.15 (dd, J = 8.1, 1.3 Hz, 1H), 8.49 (s, 1H), 8.65 (s, 1H), 9.09 (d, J = 8.5 Hz, 1H), 10.53 (s, 1H). ^{13}C NMR (75 MHz, $CDCl_3$): 196.46, 157.40, 136.64, 136.44, 133.70, 133.52, 130.75, 129.85, 128.86, 127.79, 127.32, 127.30, 127.08, 126.78, 126.37, 126.07, 125.85, 120.75, 113.97. HRMS (FAB) m/z = 272.0839, theor. calc. 272.0837 (M+). TCSPC $\tau_{1/2}$ = 2.9, 6.9 (weak) ns.

Zn^{2+} coordination compounds with (1R,2R)-(−)-1,2-diaminocyclohexane, (1S,2S)-(+)-1,2-diaminocyclohexane, (±)-trans-1,2-diaminocyclohexane and 1,2-phenylenediamine and two [4]helicene fragments (1-4). Zinc acetate (1 mmol) and diamine (1 mmol) were dissolved in 10 mL of methanol. The reaction mixture was degassed for 20 min and [4]helicene salicylaldehyde **9** (2 mmol) dissolved in 10 mL of methanol was added dropwise. The mixture was refluxed 10 minutes and stirred overnight at RT. Precipitated powders of **1-4** were

filtered and the residue washed with methanol (yields 73-95%). Protons and carbons were done by a combination of ^{1}H, ^{13}C, NOESY, COSY, HSQC and HMBC.

1 (80%)**:** ^{1}H NMR (500 MHz, DMSO-d_6): δ (ppm) 1.53 (br, 4H), 2.01 (br, 2H), 2.65 (2H), 3.45 (2H), 7.48 (d, J = 8.4 Hz, 2H), 7.66 (dd, J = 7.4 Hz, 2H), 7.88 – 7.76 (m, 6H), 7.99 (d, J = 8.5 Hz, 2H), 8.10 (d, J = 7.8 Hz, 2H), 8.14 (s, 2H), 8.29 (s, 2H), 8.75 (s, 2H), 9.25 (d, J = 8.6 Hz, 2H). ^{13}C NMR (125 MHz, DMSO-d_6): δ (ppm) 168.7, 166.1, 137.6, 135.8, 133.4, 133.1, 130.9, 129.2, 128.7, 128.6, 127.4, 126.9, 126.0, 124.4, 123.5, 122.2, 121.7, 117.1, 65.4. HRMS (FAB) m/z 684.1763, theor. 684.1755 (M+). TCSPC $\tau_{1/2}$= 1.2, 5.42 ns. **2** (73%): ^{1}H NMR (500 MHz, DMSO-d_6): δ (ppm) 1.52 (br, 4H), 2.00 (br, 2H), 2.61 (br, 2H), 3.45 (br, 2H), 7.48 (d, J = 8.6 Hz, 2H), 7.65 (dd, J = 7.2 Hz, 2H), 7.86 – 7.75z (m, 6H), 7.99 (d, J = 8.6 Hz, 2H), 8.09 (d, J = 7.8 Hz, 2H), 8.13 (s, 2H), 8.29 (s, 2H), 8.75 (s, 2H), 9.24 (d, J = 8.6 Hz, 2H). ^{13}C NMR (125 MHz, DMSO-d_6): δ (ppm) 168.4, 165.0, 137.1, 134.4, 132.8, 132.5, 130.5, 128.7, 128.2, 127.9, 127.0, 126.4, 126.3, 125.4, 124.0, 123.0, 121.6, 121.2, 116.6, 64.9, 27.7, 23.8. HRMS (MALDI) m/z 685.1828, theor. 685.1833 (M+H+). TCSPC $\tau_{1/2}$= 1.6, 6.1 ns. **3** (88%): ^{1}H NMR (500 MHz, DMSO-d_6): δ (ppm) 1.51 (br, 4H), 2.01 (br, 2H), 2.62 (2H), 3.45 (2H), 7.48 (d, J = 8.5 Hz, 2H), 7.68 (dd, J = 7.4 Hz, 2H), 7.87 – 7.76 (m, 6H), 7.99 (d, J = 8.4 Hz, 2H), 8.12 (d, J = 10.1 Hz, 2H), 8.14 (s, 2H), 8.29 (s, 2H), 8.75 (s, 2H), 9.25 (d, J = 8.5 Hz, 2H). ^{13}C NMR (125 MHz, DMSO-d_6): δ (ppm) 168.9, 165.6, 137.5, 134.8, 133.2, 132.9, 130.9, 129.2, 128.7, 128.5, 127.4, 127.0, 126.8, 125.8, 124.5, 123.4, 122.1, 121.6, 117.3, 65.3. HRMS (FAB) m/z 684.1748, theor. 684.1755 (M+). TCSPC $\tau_{1/2}$= 1.32, 5.42 ns. **4** (95%)**:** ^{1}H NMR (500 MHz, DMSO-d_6): δ (ppm) 7.50 (d, J = 8.5 Hz, 2H), 7.55 (m, 2H), 7.68 (dd, J = 7.4 Hz, 2H), 7.81 (d, J = 8.5 Hz, 2H), 7.85 (m, 4H), 8.02 (d, J = 8.5 Hz, 2H), 8.16 – 8.09 (m, 4H), 8.30 (s, 2H), 8.35 (s, 2H), 9.25 (d, J = 8.5 Hz, 2H), 9.44 (s, 2H). ^{13}C NMR (125 MHz, DMSO-d_6): 169.5, 163.9, 140.1, 138.6, 136, 133.3, 131.1, 130.9, 129.2, 128.8, 127.3, 127, 126.9, 126.1, 124.6, 123.8, 122.2, 117.6, 117.5. HRMS (FAB) m/z 678.1280, theor. 678.1286 (M+). TCSPC $\tau_{1/2}$= 1.09, 3.15 ns.

Results and discussion

Synthesis of the helicene 9

The original key building block **9** (Scheme 1) which we considered was a [4]helicene bearing an alcohol in the *ortho* position of an aldehyde group, thus reminiscent of salicylic-aldehyde, which is the proper configuration to assemble the tetradentate Schiff base. This design requires a precise stepwise construction of our precursor. For its synthesis, we have adapted procedures of phenol protection, Wittig type condensation, oxidative photocyclisation and aldehyde group formation in a multi-step procedure (Scheme 1). The synthesis consists of five steps, with good global yields.

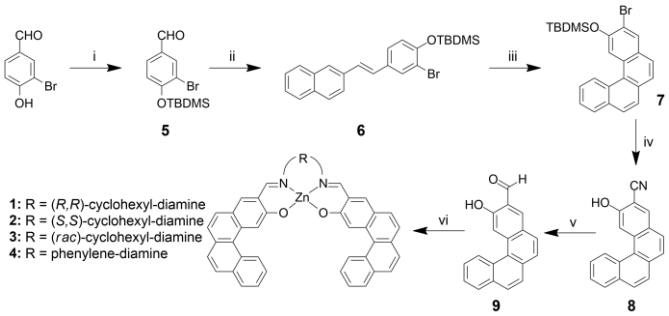

Scheme 1. Synthesis of the complexes **1**, **2**, **3** and **4**. i) TBDMSCl, imidazole, DMAP, DCM, RT, 70% ; ii) $C_{10}H_7CH_2PPh_3Br$, nBuLi, THF, -78°C to RT, 79% as a mixture of Z and E isomers; iii) hν, I_2, propylene oxide, toluene, 53% ; iv) μ-wave, CuCN, NMP, 95%; v) DIBAL-H, toluene, 53% ; vi) $Zn(OAc)_2$, diamine, MeOH, 73-95%.

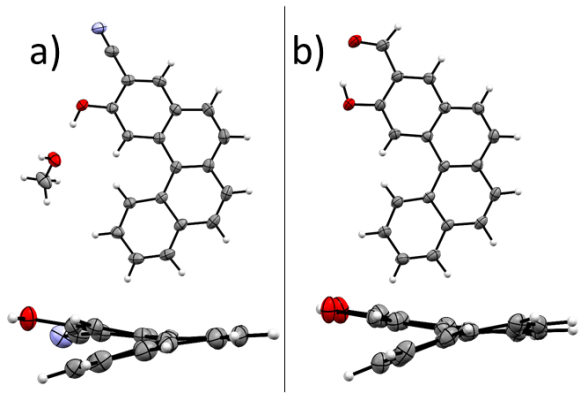

Figure 1. X-ray structures of a) compound **8** and b) compound **9**. (top : view perpendicular to the helix and bottom : side view of the helix). (Carbon: black ; Nitrogen : blue ; Oxygen : red ; Zinc : grey ; Hydrogen : white).

Although direct formylation reaction by lithium bromide exchange and addition of DMF was attempted - varying the solvents, temperature and reaction time - it yielded only the debrominated helicene. Compound **7** was therefore further reacted following a Rosenmund-von Braun reaction under microwave activation in N-methyl-pyrrolidone[39] to obtain the cyanated [4]helicene **8**. Satisfyingly, the TBDMS protecting group was simultaneously removed, presumptively because of the Lewis acid character of CuCN. The corresponding aldehyde **9** was obtained by reduction with DIBAl-H in THF.

Crystals of compound **8** suitable for X-ray analysis were obtained by slow evaporation of a $CHCl_3/CH_3OH$ solution (Fig. 1). The compound crystallized in the monoclinic space group $P2_1/n$, with one helicene and a MeOH molecule in the asymmetric unit connected by a H-bond between the two alcohol functions ($d_{O\text{-}O}$ = 2.658(1) Å). Due to the symmetry operations, both *P* and *M* enantiomers are observed in the structure. The dihedral angle in the helicene moiety is equal to

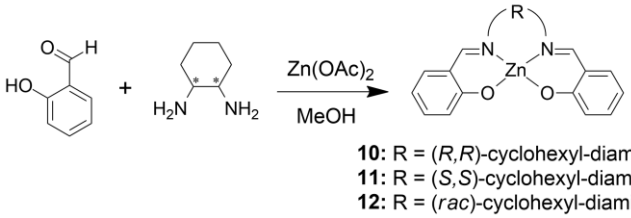

Scheme 2. Synthesis of the complexes **10**, **11**, and **12**.

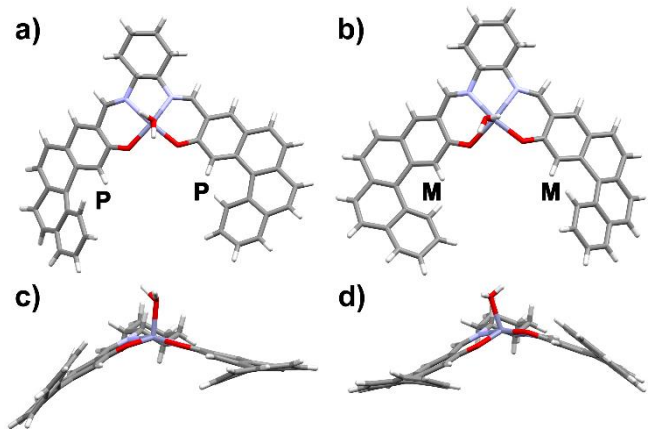

Figure 2. X-ray structure of complex **1** showing the two independent molecules from a view perpendicular to the helix axis a) for **1**-*R,R/P,P* and b) **1**-*R,R/M,M.* A view from the side of the helix is displayed c) for **1**-*R,R/P,P* and d) **1**-*R,R/M,M* (Carbon: light grey ; Nitrogen : blue ; Oxygen : red ; Zinc : grey ; Hydrogen : white).

22.5°. Compound **9**, for which single crystals have been obtained by slow diffusion of CH_3OH in a CH_2Cl_2 solution of the compound, crystallized as well in the monoclinic space group $P2_1/n$. Again, both *P* and *M* enantiomers are present in the structure. The dihedral angle between terminal benzene rings is equal to 27.1°. π–π stacking occurs between helicenes, creating enantiopure columnar stacks separated by 3.35 Å between the functionalized benzene rings. An intramolecular H-bond is observed between the alcohol hydrogen and the oxygen of the aldehyde moiety, with an O-H-O angle of 148(3)° and a O-O distance of 2.674(2) Å.

Synthesis of the complexes 1-4

Finally, the target salen complexes **1**-**4** were synthesized by a one-pot reaction with diamine, $Zn(OAc)_2$ and **9** in MeOH in good yields (Scheme 1). Model salen complexes **10**-**12**, with benzene instead of [4]helicene, were synthesized for comparison reasons according to reported literature procedures by condensation of salicyladehyde, diamine and $Zn(OAc)_2$ in MeOH (Scheme 2).[38] As assessed by single crystal X-Ray diffraction, complexes **1** and **4**, bearing two [4]helicene moieties, display the typical tetradentate O,N,N,O coordination around Zn(II) characteristic of salen ligands. Single crystals of complexes **1** and **4** were obtained by vapour diffusion of MeOH in a solution of the compound in THF at room temperature. The dataset for **1** stands below the iUCr standards despite numerous crystallization trials and an extended X-Ray irradiation time, and therefore the precise bond lengths and bond angles values will not be discussed here. Complex **1** crystallized in the non-centrosymmetric monoclinic space group *P*2. In the solid state, the Zn atom is pentacoordinated by the tetradentate O,N,N,O Schiff base and one apical water molecule in a square pyramidal conformation. Two molecules are observed in the asymmetric unit, both having two asymmetric *R,R* carbons in the cyclohexyl-diamine moiety. The first molecule displays *P,P* configuration for the helicene moiety, while the second molecule displays a *M,M* configuration (Fig. 2). They tend to associate into dyads through H-bonding interactions of the apical water molecule with their symmetrical counterparts (see the ESI). Complex **4** crystallizes in the centrosymmetric monoclinic space group $P2_1/c$ (Fig. 3). As for **1** the Zn ion is surrounded by the square defined by the tetradentate Schiff base, and bears a water molecule in its apical position. The Zn atom lies slightly above the plane formed by the four O,N,N,O atoms, thus adopting a distorted square pyramidal conformation. One molecule contains two helicene moieties with a similar configuration: either *P,P* or *M,M.* A THF molecule completes the structure. *P,P* and *M,M* molecules are connected by four hydrogen bonds between the hydrogens of the apical water molecule and the oxygens of the salen moiety, with O···O distances in the 2.6-2.7 Å range, and O-H-O angles of 129° and 152°.

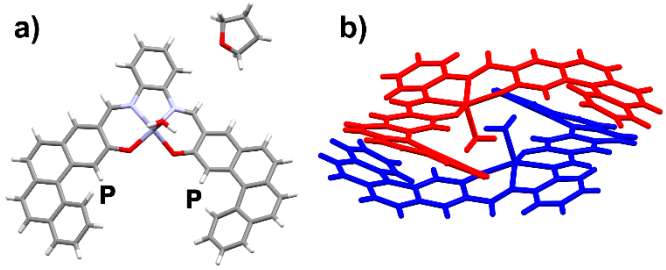

Figure 3. X-ray structure of complex **4**. a) Asymmetric unit and b) H-bonded dimer observed in the solid state (*M,M* complex : red ; *P,P* complex : blue).

Spectroscopic properties

UV-visible spectra of the complexes were measured in THF solutions at 10^{-5} M and were compared with the theoretical spectra resulted from TD-DFT calculations using Gaussian with the PBE1PBE functional and a def2SVP basis set. The X-ray structure was used as a basis for atomic positions, which were further optimized. Experimentally, for complexes **1-3** wide absorption band are observed with maxima at 273 nm (ε = 60000 $L{\cdot}mol^{-1}{\cdot}cm^{-1}$), 322 nm (ε = 78000 $L{\cdot}mol^{-1}{\cdot}cm^{-1}$) and 350 nm (ε = 38000 $L{\cdot}mol^{-1}{\cdot}cm^{-1}$) which can be attributed to π–π* transitions in the aromatic moieties. Both the position and the overall ε values are in good agreement with the calculations. A further broad absorption band is observed for complexes **1-3** at 454 nm (ε = 6500 $L{\cdot}mol^{-1}{\cdot}cm^{-1}$), which can be attributed to an ILCT character. The UV spectrum of complex **4** is much less structured, owing to the presence of the extra phenyl rings of the diamine and in this case the most red-shifted absorption is found at 483 nm (ε = 3700 $L{\cdot}mol^{-1}{\cdot}cm^{-1}$). HOMO and LUMO orbitals, calculated for **1** in the *R,R/M,M* configuration, involved in this low energy transition, are represented in Fig. 4f. It is worth noting that for both *R,R/M,M* and *R,R/P,P* configurations HOMO-1/HOMO and LUMO/LUMO+1 are degenerated and participate in both the S1 and S2 transitions (ESI). The electron density difference maps (Fig. 4f) between S1-S0 and S2-S0 are helpful here to understand the transitions, which are mostly consisting of a transfer of electronic density involving the salen and the helicene units. The difference in stability between the two diastereomers is not big enough to hypothesize that a helicene configuration would be favored in solution.

For all complexes **1**-**4** the excitation spectrum is very similar to the absorption one, whereas the emission for **1**-**3** has a maximum at 550 nm and for **4** at 620 nm (Fig. 4b and ESI).

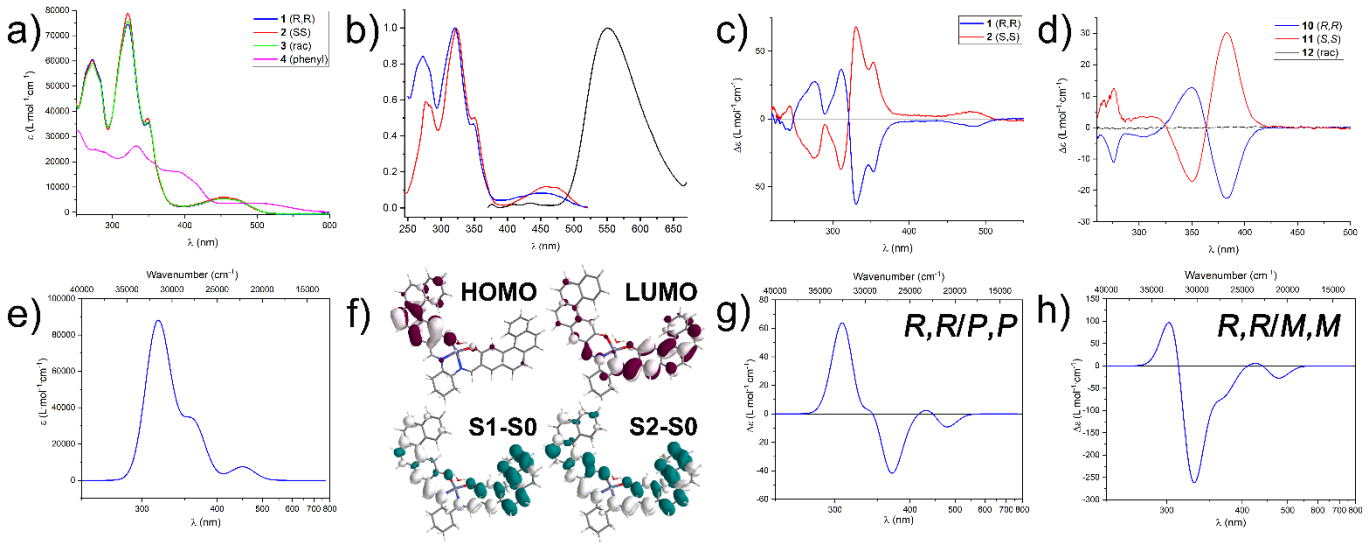

Figure 4. UV-visible spectra of the a) complexes **1-4** (THF, 10^{-5} M), b) normalized emission and excitation spectra (λ_{em} = 350 nm ; λ_{exc} = 530 nm) of complex **3** (THF, 10^{-5} M range, blue: absorption ; red: excitation ; black : emission), c) ECD spectra of complexes **1** and **2** (THF, 1-1.5·10^{-5} M range), d) ECD spectra of model complexes **10**-**12** (DMSO, 2-3.10^{-5} M range), e) calculated UV-visible spectra for complex **1**, f) frontier molecular orbitals of **1** and representation of the Electron Density Difference (S1-S0 - left) and (S2-S0 - right), calculated circular dichroism spectra for complex **1** with helicene moieties in the g) *P,P* and h) *M,M* conformations.

Complexes **1-3** have moderate quantum yields in the 10-16% range, while the phenyl derivative **4** displays only a 2.5% quantum yield (using quinine sulfate in 0.1M H_2SO_4 as a reference). Two lifetimes are displayed for each complex: a first one in the 1-1.6 ns range, and a second one of 3.1 ns (complex **4**) and around 5.4-6.0 ns for complexes **1-3** (Table S1 in the ESI), all properly fitted to the experimental time correlated single photon counter (TCSPC) values using a bi-exponential function. The obtained values are in accordance with previously reported data, and could be explained by the competition between a π^*-π and a CT transition.[40,41] The excitation spectra present a perfect match with the absorption spectra for the four complexes (Fig. 4b and ESI).

Chiroptical properties

Thanks to the chiral diamine moiety, the complexes **1** and **2** are active in circular dichroism (Fig. 4c). For the sake of comparison, in order to disclose between a possible participation of the [4]helicene moieties and that of the chiral salen complex to the CD spectra, chiroptical properties of complexes **10** and **11** have been measured as well. They display a relatively strong response in CD (Fig. 4d). Interestingly, the charge transfer band involving the aromatics in the helicene moiety around 450-500 nm is CD active, with $\Delta\varepsilon$ of -5 L·mol^{-1}·cm^{-1} for **1** and 5 L·mol^{-1}·cm^{-1} for **2** at 480 nm, very likely resulting from an exciton coupling between the two helicene chromophores. Based on the structure of (*R,R*)-diaminocyclohexane, one can predict a negative couplet, with a crossover point at about 454 nm, a negative band at longer wavelengths and a positive one at shorter ones.[42] This is indeed found in the experiment, where the positive component of the couplet is cancelled by the negative tail of the 330-360 nm system of CD bands. In the calculations (Fig. 4g and 4h and ESI) this couplet is much more evident. The ECD bands around 450-500 nm are absent in the model complexes **10** and **11**, which supports the active part taken by the extended aromatic moieties of **1** and **2** in the CD spectra. In the calculated CD spectra for **1**-*R,R/P,P* and **1**-*R,R/M,M*, the sign of the transitions above 400 nm does not change with the helicity of the aromatic part, *i.e.* it is mostly dictated by the chirality of the stereogenic centers of the cyclohexyl-diamine moiety. Furthermore, stronger signals with maxima at 353 and 330 nm are observed for **1** and **2**, with $\Delta\varepsilon$ absolute values of 39 and 63 L·mol^{-1}·cm^{-1} respectively.

CPL associated to Zn-salen helicene compounds **1-2** was easily recorded thanks to a strong total luminescence and the absence of any significant photoselection. Complexes **1** and **2** display clear mirror image CPL signals with a maximum around 535 nm, retracing the fluorescence spectrum (Fig. 5). Dissymmetry factors g_{lum} around +1.3·10^{-3} and -1.6·10^{-3} were obtained at 535 nm for the *S,S* and *R,R* enantiomers, respectively. The sign is consistent with that observed for low energy ECD transitions (below 320 nm). The magnitude of the g_{lum} factors is in the usual range for transition metal complexes containing helicene units. Similarly, Zn-salen models **10** and **11** compounds show mirror image CPL signals with a maximum around 440 nm, retracing the fluorescence spectrum. Dissymmetry factors around +1.1·10^{-3} and -1.3·10^{-3}, thus only slightly lower than the helicenic complexes, were obtained at 440 nm for the *S,S* and *R,R* enantiomers, respectively. Again, the sign is consistent with the one of the most red-shifted ECD transitions.

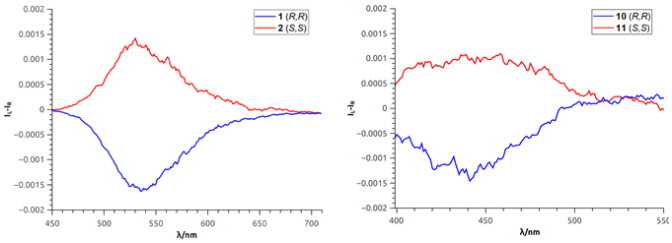

Figure 5. CPL spectra of (left) compounds **1-2** (~1·10^{-1} M in THF, λ_{exc} = 365 nm) and (right) model compounds **10-11** (~1·10^{-1} M in DMSO, λ_{exc} = 365 nm).

The dissymmetry factors obtained in both cases are in line with previous reports on Zn-salen CPL.[20] The CPL brightness defined by **Equation 1** was calculated [43]:

Equation 1 : $B_{CPL} = \frac{\varepsilon \times \Phi \times |g_{lum}|}{2}$

Complexes **1**, **2, 10** and **11** have B_{CPL} of 1.2, 0.8, 1.8 and 1.3 $L{\cdot}mol^{-1}{\cdot}cm^{-1}$ respectively. This places **1** and **2** below the average organic helicene values of 18.7 $L{\cdot}mol^{-1}{\cdot}cm^{-1}$ for CPL brightness, but on the high side of the range of the reported average values for *d*-Metal based compounds, which are 0.14, 0.79 and 1.0 $L{\cdot}mol^{-1}{\cdot}cm^{-1}$ for Re(I), Ir(III) and Pt(II) complexes respectively.[43]

Conclusions

In summary, we reported here the first synthesis and characterization of Schiff base Zn(II) complexes incorporating a helicenic scaffold. They exhibit excellent optical properties as fluorescent materials and display chiroptical activity.

The stereochemistry imposed by the chiral diamine is partially transferred to the helicene scaffold in solution and observed in electronic circular dichroism. Bi-exponential decrease of the luminescence lifetime is observed with two lifetimes in the range of 1-2 and 5-6 ns, respectively along with a QY in the 15% range. CPL is in the expected range for the emission wavelength and intensity for the complexes as attested by the B_{CPL} values. The sign of the CPL signal is determined by the chirality of the diamine employed in the synthesis. Theoretical calculations support the observed optical properties. These Zn(salen) complexes could be explored for their chiral electroluminescence properties in the visible.[38] Extending the size of the helicene moiety to block its configuration is the most important development, which is underway in our groups.

Author Contributions

M.S., S.V. and N.Z. performed the synthesis and spectroscopic characterizations, T.C. did the theoretical calculations, M.L. executed TC-SCP measurements, F.Z. and L.D.B carried out CPL measurements, and N.Z. and N.A. supervised the project and wrote the manuscript with input from all the co-authors.

Conflicts of interest

There are no conflicts to declare.

Acknowledgements

The RFI LUMOMAT network is thanked for the training fellowship of M. Savchuk and S. Vertueux. CNRS and University of Angers are acknowledged for their financial support.
M. Mastropasqua and M. Allain (MOLTECH-Anjou, University of Angers) are thanked for helpful discussions.

Notes and references

‡ Electronic Supplementary Information (ESI) available. CCDC 2080966–2080969. For ESI and crystallographic data in CIF or other electronic format see DOI: 10.1039/x0xx00000x

1 P. G. Cozzi, *Chem. Soc. Rev.*, 2004, **33**, 410–421.
2 C. J. Whiteoak, G. Salassa and A. W. Kleij, *Chem Soc Rev*, 2012, **41**, 622–631.
3 R. M. Clarke and T. Storr, *Dalton Trans.*, 2014, **43**, 9380.
4 W. Zhang, J. L. Loebach, S. R. Wilson and E. N. Jacobsen, *J. Am. Chem. Soc.*, 1990, **112**, 2801–2803.
5 T. Katsuki, *Adv. Synth. Catal.*, 2002, **344**, 131–147.
6 H. Miyasaka, A. Saitoh and S. Abe, *Coord. Chem. Rev.*, 2007, **251**, 2622–2664.
7 M. Andruh, *Chem. Commun.*, 2011, **47**, 3025–3042.
8 I. Ramade, O. Kahn, Y. Jeannin and F. Robert, *Inorg. Chem.*, 1997, **36**, 930–936.
9 M. Andruh, *Dalton Trans.*, 2015, **44**, 16633–16653.
10 B. J. Kennedy and K. S. Murray, *Inorg. Chem.*, 1985, **24**, 1552–1557.
11 H. Miyasaka, T. Madanbashi, K. Sugimoto, Y. Nakazawa, W. Wernsdorfer, K. Sugiura, M. Yamashita, C. Coulon and R. Clérac, *Chem. – Eur. J.*, 2006, **12**, 7028–7040.
12 H. Miyasaka, K. Takayama, A. Saitoh, S. Furukawa, M. Yamashita and R. Clérac, *Chem. – Eur. J.*, 2010, **16**, 3656–3662.
13 C.-M. Che, C.-C. Kwok, S.-W. Lai, A. F. Rausch, W. J. Finkenzeller, N. Zhu and H. Yersin, *Chem. – Eur. J.*, 2010, **16**, 233–247.
14 Y. Hai, J.-J. Chen, P. Zhao, H. Lv, Y. Yu, P. Xu and J.-L. Zhang, *Chem. Commun.*, 2011, **47**, 2435–2437.
15 G. S. M. Tong, P. K. Chow, W.-P. To, W.-M. Kwok and C.-M. Che, *Chem. – Eur. J.*, 2014, **20**, 6433–6443.
16 X. Yang, R. A. Jones and S. Huang, *Coord. Chem. Rev.*, 2014, **273–274**, 63–75.
17 G. Yu, Y. Liu, Y. Song, X. Wu and D. Zhu, *Synth. Met.*, 2001, **117**, 211–214.
18 O. Lavastre, I. Illitchev, G. Jegou and P. H. Dixneuf, *J. Am. Chem. Soc.*, 2002, **124**, 5278–5279.
19 A. C. W. Leung, J. H. Chong, B. O. Patrick and M. J. MacLachlan, *Macromolecules*, 2003, **36**, 5051–5054.
20 Y. Chen, X. Li, N. Li, Y. Quan, Y. Cheng and Y. Tang, *Mater. Chem. Front.*, 2019, **3**, 867–873.
21 F. Pop, N. Zigon and N. Avarvari, *Chem. Rev.*, 2019, **119**, 8435–8478.
22 Y. Shen and C.-F. Chen, *Chem. Rev.*, 2012, **112**, 1463–1535.
23 M. Gingras, *Chem. Soc. Rev.*, 2013, **42**, 1051–1095.
24 K. Dhbaibi, L. Favereau and J. Crassous, *Chem. Rev.*, 2019, **119**, 8846–8953.
25 J. R. Brandt, X. Wang, Y. Yang, A. J. Campbell and M. J. Fuchter, *J. Am. Chem. Soc.*, 2016, **138**, 9743–9746.
26 Z. Yan, X. Luo, W. Liu, Z. Wu, X. Liang, K. Liao, Y. Wang, Y. Zheng, L. Zhou, J. Zuo, Y. Pan and H. Zhang, *Chem. – Eur. J.*, 2019, **25**, 5672–5676.
27 E. S. Gauthier, L. Abella, N. Hellou, B. Darquié, E. Caytan, T. Roisnel, N. Vanthuyne, L. Favereau, M. Srebro-Hooper, J. A. G. Williams, J. Autschbach and J. Crassous, *Angew. Chem. Int. Ed.*, 2020, **59**, 8394–8400.
28 T. Biet, A. Fihey, T. Cauchy, N. Vanthuyne, C. Roussel, J. Crassous and N. Avarvari, *Chem. – Eur. J.*, 2013, **19**, 13160–13167.
29 T. Biet, T. Cauchy, Q. Sun, J. Ding, A. Hauser, P. Oulevey, T. Burgi, D. Jacquemin, N. Vanthuyne, J. Crassous and N. Avarvari, *Chem. Commun.*, 2017, **53**, 9210–9213.

30 T. Biet, K. Martin, J. Hankache, N. Hellou, A. Hauser, T. Bürgi, N. Vanthuyne, T. Aharon, M. Caricato, J. Crassous and N. Avarvari, *Chem. – Eur. J.*, 2017, **23**, 437–446.
31 A. Abhervé, K. Martin, A. Hauser and N. Avarvari, *Eur. J. Inorg. Chem.*, 2019, **2019**, 4807–4814.
32 F. Zinna, T. Bruhn, C. A. Guido, J. Ahrens, M. Bröring, L. Di Bari and G. Pescitelli, *Chem. - Eur. J.*, 2016, **22**, 16089–16098.
33 M. J. Frisch, G. W. Trucks, H. B. Schlegel, G. E. Scuseria, M. A. Robb, J. R. Cheeseman, G. Scalmani, V. Barone, B. Mennucci, G. A. Petersson, H. Nakatsuji, M. Caricato, X. Li, H. P. Hratchian, A. F. Izmaylov, J. Bloino, G. Zheng, J. L. Sonnenberg, M. Hada, M. Ehara, K. Toyota, R. Fukuda, J. Hasegawa, M. Ishida, T. Nakajima, Y. Honda, O. Kitao, H. Nakai, T. Vreven, J. A. Montgomery Jr., J. E. Peralta, F. Ogliaro, M. Bearpark, J. J. Heyd, E. Brothers, K. N. Kudin, V. N. Staroverov, R. Kobayashi, J. Normand, K. Raghavachari, A. Rendell, J. C. Burant, S. S. Iyengar, J. Tomasi, M. Cossi, N. Rega, J. M. Millam, M. Klene, J. E. Knox, J. B. Cross, V. Bakken, C. Adamo, J. Jaramillo, R. Gomperts, R. E. Stratmann, O. Yazyev, A. J. Austin, R. Cammi, C. Pomelli, J. W. Ochterski, R. L. Martin, K. Morokuma, V. G. Zakrzewski, G. A. Voth, P. Salvador, J. J. Dannenberg, S. Dapprich, A. D. Daniels, Ö. Farkas, J. B. Foresman, J. V. Ortiz, J. Cioslowski and D. J. Fox, *Gaussian~09 Revision D.01*, .
34 C. Adamo and V. Barone, *J. Chem. Phys.*, 1999, **110**, 6158–6170.
35 F. Weigend and R. Ahlrichs, *Phys. Chem. Chem. Phys.*, 2005, **7**, 3297.
36 F. B. Mallory, C. W. Mallory and W. M. Ricker, *J. Org. Chem.*, 1985, **50**, 457–461.
37 R. Tello-Aburto and A. M. Harned, *Org. Lett.*, 2009, **11**, 3998–4000.
38 F. Dumur, L. Beouch, M.-A. Tehfe, E. Contal, M. Lepeltier, G. Wantz, B. Graff, F. Goubard, C. R. Mayer, J. Lalevée and D. Gigmes, *Thin Solid Films*, 2014, **564**, 351–360.
39 J. Žádný, P. Velíšek, M. Jakubec, J. Sýkora, V. Církva and J. Storch, *Tetrahedron*, 2013, **69**, 6213–6218.
40 I. Majumder, P. Chakraborty, S. Dasgupta, C. Massera, D. Escudero and D. Das, *Inorg. Chem.*, 2017, **56**, 12893–12901.
41 D. Majumdar, S. Das, R. Thomas, Z. Ullah, S. S. Sreejith, D. Das, P. Shukla, K. Bankura and D. Mishra, *Inorganica Chim. Acta*, 2019, **492**, 221–234.
42 N. Berova, L. D. Bari and G. Pescitelli, *Chem. Soc. Rev.*, 2007, **36**, 914–931.
43 L. Arrico, L. Di Bari and F. Zinna, *Chem. – Eur. J.*, 2021, **27**, 2920–2934.